Second-order transition in Rochelle-salt saturated solutions

Horia V. Alexandru
Laboratory for Materials Science and Crystal Growth, University of Bucharest, National Center of Physics, Bucharest-Magurele, Romania

(Received 8 April 1991; revised manuscript received 30 December 1991)

A *sui generis* second-order transition in water solutions of Rochelle-salt crystal has been seen during measurements of both the solubility and solution densities versus temperature. Both the volume-expansion coefficients and the temperature differential of solution densities for several compositions along the solubility curve present a jump discontinuity around a saturation temperature of 24 °C. Electrical measurements revealed a small peak in the dielectric constant, showing a minute ferroelectric component of solute near 24 °C in solution. The loss tangents of solution and the dissolution enthalpy (drawn from the solubility curve) show other characteristics. The excess volume of solute vanishes around 31 °C, showing an "ideal" behavior of solution in this region. All data seem to indicate the tartrate molecule $NaKC_4H_4O_6$ associates with the four water molecules in solution, just like the water molecules undergoing crystallization. This quasicrystalline structure of the solute is stable in solutions up to about 40 °C. A tentative interpretation as a critical phenomenon is made for the volume-expansion coefficient. This response function with a cusplike singularity at 24 °C has a critical point exponent of about $\frac{1}{2}$. A one-to-one correspondence within four temperature ranges (between 16–18 °C and 58 °C), of the properties of the crystal and solute Rochelle salt, has been experimentally proved in five types of measurements.

PACS number(s): 05.70.Fh, 64.70.−p, 64.80.−v, 64.90.+b

I. INTRODUCTION

Large Rochelle-salt (RS) single crystals have been grown from solutions [1,2]. Growth kinetics [3], size distributions [4], and critical growth rates [2,5,6] were measured.

Solubility data of RS in water have been drawn from Refs. [7] and [8] and checked in several growth experiments [1–3]. Previous experiments of density measurements [9] gave evidences for an unusual transition in RS solutions around 24 °C. This temperature is the Curie point of the ferroelectric transition of the solute in its solid state.

Measurements of the solubility and the solution density versus temperature for different compositions were performed to find some reliable correlations for the precise determination of the saturation temperature during growth experiments of the RS crystal with fewer possible perturbations. Some other regularities were discerned in subsequent experiments, which shall be presented in this paper.

II. EXPERIMENT

The experiments setup we used was a modified version of the equipment for growth-kinetics measurements as described previously [10]. In brief, a double-walled thermostated system (10-l cylindrical vessel and inner four-necked 2.5-l glass vessel) ensured, under continuous stirring, the temperature control in the outer shirt of distilled water within ±0.02 °C. A heating element of 300-W maximum adjustable power was monitored by a contract thermometer and an electronic relay. The whole thermostated system has been placed on a specially designed electric stove that could deliver a constant adjustable power.

The saturated solutions were prepared starting with 1000 g bidistilled water and analytical-grade Rochelle salt. Every new composition has been obtained by adding the estimated solute difference to the previous solution according to the solubility curve [7,8]. At least 12 compositions have been produced. Every saturation temperature has been carefully tested (±0.02 °C accuracy) using a previously grown crystal and the weighing method.

A rasotherm (Jena) glass diver has been calibrated versus the water density [11], according to the formula

$$\rho^{\mathrm{div}}=\left[1-\frac{m'}{m_0}\right]^{-1}\rho_{\mathrm{water}}\ , \tag{1}$$

where m_0 is the diver mass measured in air and m' is the apparent mass of the diver in water.

For a 20–40 °C temperature range, $\rho^{\mathrm{div}}=2.223_8$ g/cm^3 with a precision as defined by Pratten [12] of $\pm 2\times 10^{-4}$ g/cm^3, and for a larger temperature range, 10–60 °C of maximum $\pm 5\times 10^{-4}$ g/cm^3 (this largely covers both the weighing error $\pm 1\times 10^{-4}$ g and those due to the diver-volume expansion).

The calibrated diver has been suspended with a nylon thread with diameter 0.15 mm from a scale of an analytical balance and for any solution composition C_S (g solute/100 g H_2O), the density has been calculated versus temperature

$$\rho^{\mathrm{sol}}(T)=\left[1-\frac{m''(T)}{m_0}\right]\rho^{\mathrm{div}}\ , \tag{2}$$

where $m''(T)$ is the apparent mass of the diver in solution.

 ©1992 The American Physical Society

Double-walled tubes (with diameters 12 and 24 mm, 15 cm in length), through which both nylon wires of the diver and of the crystal penetrate, were fitted in the central rubber stopper of the inner vessel containing the solution. They prevent solvent evaporation and heat exchange. Besides, the top covers of these tubes provided with narrow holes for nylon penetration have improved the temperature stability.

A set of measurements was performed over about 10–14 h. The inner solution vessel was sealed between the successive runs and the system was thermostated close to the saturation point of the solution. For $T<31\,^{\circ}\mathrm{C}$ no preheating of solutions was performed before each set of density measurements. Usually each solution composition was changed just before the measurement run.

III. RESULTS

The densities of the solutions versus temperature for several compositions (marked by the saturation temperature T_S), are presented in Fig. 1. No change of the density slope versus temperature has been recorded crossing up and down 5–10 °C the saturation point.

The least-squares method has been used to fit the data for a given concentration

$$\rho(T)=\rho_0+\left[\frac{d\rho}{dT}\right]_{T_S}T,\quad \frac{d\rho}{dT}<0 \tag{3}$$

with a correlation factor better than 99.8%. The volume-expansion coefficients α_s and α_0 have been calculated according to the formulas

$$\alpha_s=\frac{1}{V}\left[\frac{dV}{dT}\right]_{T_S}=-\frac{1}{\rho_s}\left[\frac{d\rho}{dT}\right]_{T_S}, \tag{4}$$

$$\alpha_0=-\frac{1}{\rho_0}\left[\frac{d\rho}{dT}\right]_{T=0\,^{\circ}\mathrm{C}}. \tag{5}$$

The density values calculated at the saturation temperature according to Eq. (3) are in close agreement with those experimentally found within 5×10^{-5} g/cm^3.

All important data have been collected in Table I. Solubilities $C_S(T)$ (in g solute/100 g H_2O) are in good agreement with other data [7,8]. Small deviations in solubility have been recorded due to solvent evaporation during the 14 days of measurements. After about a 12-h rest of the solution at $T=38.9\,^{\circ}\mathrm{C}$, a 0.05 °C increase of the saturation temperature has been recorded between two successive runs. For two other successive runs and a 20-h rest at $T=42.5\,^{\circ}\mathrm{C}$ the increase of the saturation was about 0.08 °C. Double runs have been performed at that temperature in order to check the reproducibility of the data. Deviations smaller than 2% could be recorded for α_s, α_0, and $(d\rho/dT)_{T_S}$ in Table I, Nos. 10 and 11.

The most important data are presented in Fig. 2. Both α_s and $(d\rho_s/dT)_{T_S}$ calculated along the solubility curve

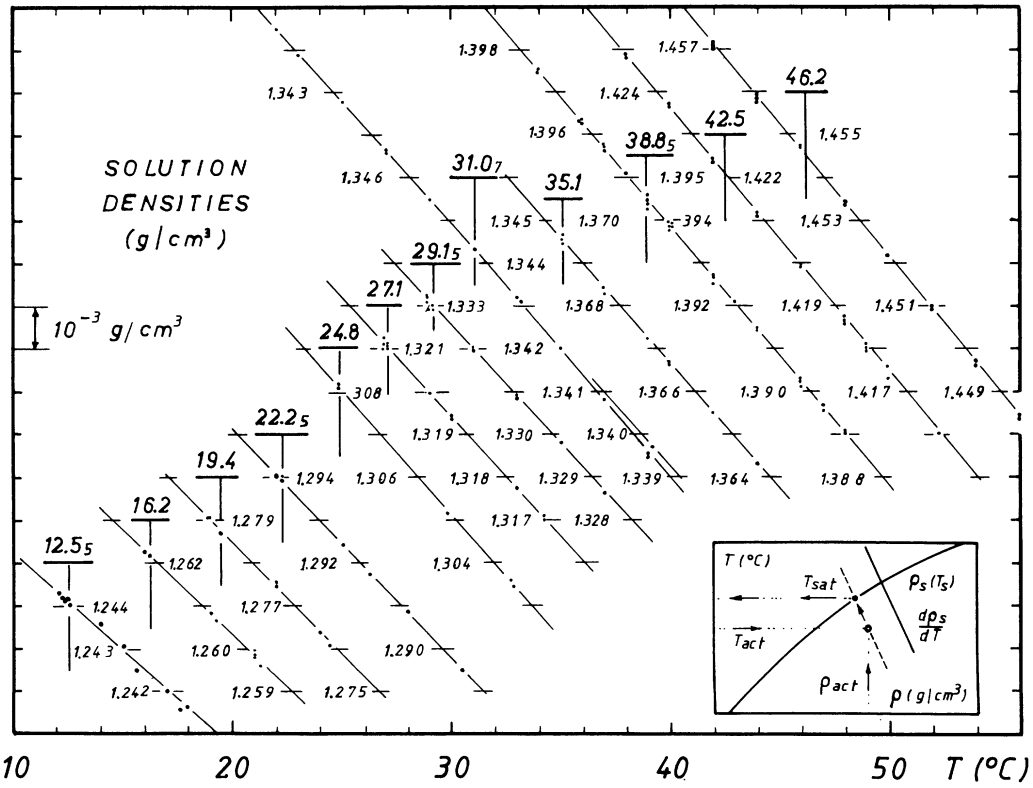

FIG 1. Solution densities vs temperature and composition. The saturation temperatures for the different compositions are recorded on the top of the vertical bars. The density scale in the ordinate axis is floating for different compositions. Inset—the procedure for the saturation temperature determination.

TABLE I. The main characteristic data of Rochelle-salt water solutions.

Expt. No.	T_{sat} (°C)	C_S[a] (g/100 g H_2O)		ρ_{sat}^{meas} (g/cm^3)	ρ_0^{calc} (g/cm^3)	$10^5\alpha_s$ (°C^{-1})	$10^5\alpha_0$ (°C^{-1})	$10^5\left\|\frac{d\rho}{dT}\right\|$ (g/cm^3 K)
1	12.55	75.0		1.244_{10}	1.250_{02}	37.9_4	37.7_6	47.2
2	16.20	85.5	[85]	1.262_{20}	1.270_{20}	39.0_6	38.8_1	49.3
3	19.40	95.5	[95]	1.278_{70}	1.288_{70}	40.7_4	40.4_3	52.1
4	22.25	105.0	[105]	1.294_{00}	1.306_{24}	42.5_8	42.1_8	55.1
5	24.80	115.0	[115]	1.308_{15}	1.322_{54}	44.3_4	43.8_5	58.0
6	27.10	125.0	[125]	1.321_{12}	1.336_{36}	42.6_9	42.2_0	56.4
7	29.15	135.5	[135]	1.333_{00}	1.349_{04}	41.2_6	40.7_7	55.0
					1.349_{44}	42.1_6	41.6_5	56.2
8	31.07	146.6	[145]	1.344_{45}	1.362_{21}	42.1_7	41.6_2	56.7
						42.5_4	41.9_9	57.2
9	35.10	174.3	[170]	1.369_{55}	1.390_{01}	42.5_7	41.9_4	58.3
10	38.85	206.8	[200]	1.394_{55}	1.418_{05}	43.3_8	42.6_6	60.5
	38.90		[200]	1.394_{85}	1.418_{07}	42.8	42.1	59.7
11	42.50	246.8	[240]	1.422_{15}	1.448_{64}	43.8_8	43.0_7	62.4
						43.3_8	42.6	61.7
	42.58		[240]	1.422_{65}	1.448_{61}	42.9_5	42.1_8	61.1
12	46.20	310	[300]	1.454_{55}	1.483_{24}	42.6_9	41.8_7	62.1

[a]Figures in square brackets experimentally used are not entirely correct due to solvent evaporation—see text. Up to $T \simeq 30$ °C our data remain correct within experimental errors.

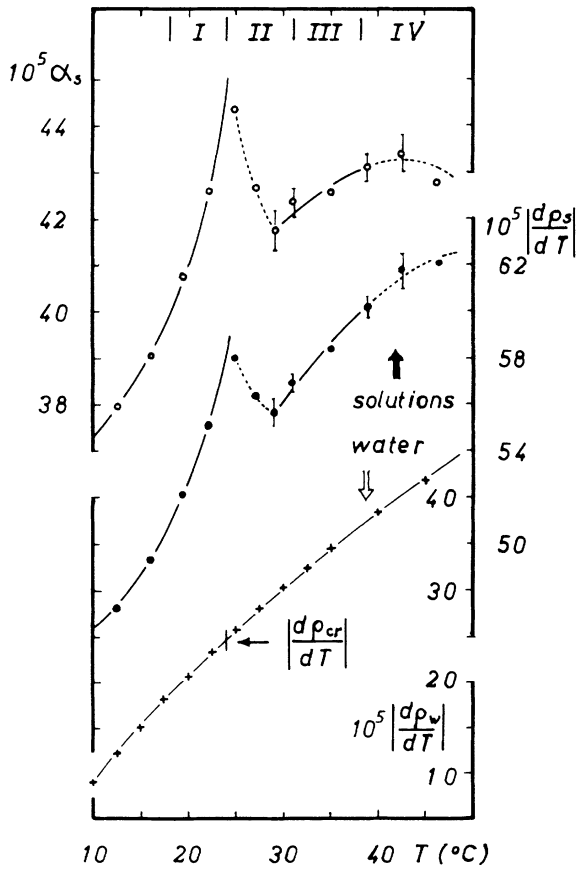

FIG. 2. The volume-expansion coefficient and the temperature differential of solution density vs the saturation temperature. The lower smooth curve $|d\rho_w/dT|$ for pure water stands for comparison. $|d\rho_{cr}/dT|_{24\,°C} = |d\rho_w/dT|_{24\,°C}$.

have a jump discontinuity around 24 °C saturation temperature. For pure water ($d\rho_w/dT$), which we have calculated [11] to make a comparison, is smooth around that temperature.

A large graph of solution density at saturation $\rho_s(T_S)$ and the temperature differential $(d\rho_s/dT)_{T \gtrless T_S}$ around the saturation points has been drawn to be put into practice. During subsequent RS crystal-growth experiments the saturation temperature at different stages could be estimated within ±0.1 °C accuracy. A Mohr-Westphal balance of accuracy $\pm 2 \times 10^{-4}$ g/cm^3 calibrated for this purpose was used to measure the solution density at the actual growing temperature $T \leq T_S$ (inset in Fig. 1).

IV. DISCUSSION OF THE METHOD

The data obtained using this method are at least competitive with similar data obtained for a triglycine sulfate (TGS) crystal [13]. The main sources of errors in the density measurements were the minute water droplets adherent to the nylon wire during the diver calibration, air bubbles adherent to the diver surface in water or solutions, and the diver expansion, especially for higher-temperature measurements. Every caution has been taken to avoid these errors.

On the temperature range $T_S \pm 10$ °C the undersaturation value of the volume-expansion coefficient $\alpha_s^{T > T_S}$ is less than 2% smaller than the supersaturation one value $\alpha_s^{T < T_S}$. In Fig. 1, for instance, $T_S = 31.07$ °C, $\alpha_s^{T > T_S} = 42.1_7 \times 10^{-5}$ °C^{-1}, $\alpha_s^{T < T_S} = 42.5_4 \times 10^{-5}$ °C^{-1}. This is not actually related to a crossing of the saturation temperature effect, but merely due to the fact that α_s has in its turn a weak dependence of temperature.

Three types of corrections have to be considered: (a) a vacuum weighing correction which amounts to a maximum solution-density error of -2.5×10^{-4} g/cm^3; (b) a nylon Archimedean force in solution (and water); and (c) a surface-tension effect of solution (or water) on the nylon thread. This last correction does not exceed 5×10^{-4} g/cm^3 and has an opposite sign to the (b) correction. These corrections partly compensate each other. On the other hand, only relative solution-density measurements have been performed versus the water density. So we estimate the absolute density error to be $\pm5\times10^{-4}$ g/cm^3 at most.

V. CRYSTAL-DENSITY MEASUREMENTS

Every solution composition had its own saturation test, joint to a set of solution-density measurements. A RS single crystal of 10–20 g has been used for this purpose. The density of these test RS crystals has been determined versus the saturation temperature of the solutions,

$$\rho^{\mathrm{cr}}(T_S)=\left[1-\frac{m'_{\mathrm{cr}}}{m_{\mathrm{cr}}}\right]^{-1}\rho^{\mathrm{sol}}(T_S)\ . \tag{6}$$

These values have been fitted between 20 and 46 °C by the equation

$$\rho^{\mathrm{cr}}(T)=1.773_{33}-19.5\times10^{-5}T\ (^\circ\mathrm{C}) \tag{7}$$

using the least-squares method, with a correlation factor 97.4%.

Unfortunately, to measure the crystal density by this method is not accurate enough. First, because the saturation point could not be reached instantaneously, and this increases the m'_{cr} error determination. Second, because the moist crystal, drawn from solution, or the crystal after drying in atmosphere, has apparently the larger m_{cr}. The errors are much larger than the weighing precision.

On the other hand, the slight dissolution or growth of the test crystal—usually less than 0.1 g—does not disturb the saturation point stability of solutions. RS crystal density and its volume-expansion coefficient that we have calculated from other literature data are presented in Table II.

VI. CRYSTAL-DENSITY DISCUSSIONS

We have used the x-ray data from Refs. [14] and [15] to calculate the crystal density. The most probable value at 20° is $\rho_{\mathrm{cr}}^{20^\circ\mathrm{C}}=1.772$ g/cm^3 (see Nos. 1, 2, and 6 in Table II). Incidentally, using the Beevers and Hughes cell parameters [15], but $c=6.20$ Å instead of 6.16 Å ($c=6.20$ Å is the Staub value [14]), the mentioned figure has been obtained for the crystal density.

The density value we have calculated in Table II (No. 3), following the Ubbelohde and Woodward x-ray data [14] is some 0.75% larger than 1.772 g/cm^3. Although more accurate (about one order of magnitude) than previous x-ray data, the smaller values reported for the cell parameters [14] seem to be due to the crystallization water loss. This is suggested by the whitening of the minute crystals (~1 mm) that were noticed [14] during measurements. Indeed, according to Vignes [16], even under an impervious coating, after a long exposure to an x-ray beam a RS crystal loses the crystallization water.

The volume-expansion coefficient of the RS crystal that we have calculated following the literature data [14–18] (presented in Table II) is about $\frac{1}{3}$ of that of the saturated solutions in Fig. 2. The linear-expansion coefficient a_1 along the ferroelectric axis of the crystal, measured by Imai [17], is presented in the lower inset of Fig. 3. It shows the discontinuity around the Curie point. However, the jump anomaly of the volume-expansion coefficient of the crystal, at the upper Curie point, is only -0.14×10^{-5} °C^{-1} (i.e., only 1% decrease), because the other two linear coefficients a_2 and a_3 have smaller, but positive, jumps.

We have fitted the most reliable data of Jona [18,19] about the RS crystal density with the equation

$$\rho^{\mathrm{cr}}(T)=1.776_{88}-22.8\times10^{-5}T\ (^\circ\mathrm{C}) \tag{8}$$

in order to use them in further calculations.

The volume-expansion coefficient of the crystal we have calculated following the Imai data (Fig. 3 in Ref. [17]), between 0 and 24 °C, can be represented by

$$\alpha_v^{0-24}=14.1_7\times10^{-5}+2.7_5\times10^{-7}T\ (^\circ\mathrm{C})\ . \tag{9}$$

TABLE II. Rochelle-salt crystal density and the volume-expansion coefficient.

Expt. No.	$\rho^{20^\circ\mathrm{C}}/\rho^{35^\circ\mathrm{C}}$ (g/cm^3)	$10^5\alpha_s$ (°C^{-1})	Refs.
1	1.772_5		Staub [14], x rays
2	1.780_7		Beevers and Hughes [15], x rays
	1.772_{05} for $c=6.20$ Å		See text, x rays
3	$1.785_7/1.781_4$	$\alpha^{-50+20}=13.7_6$	Ubbelohde and Woodward [14], x rays
		$\alpha^{+20+35}=16.2_3$	
4		$\alpha^{+12+24}=13.5_9$	Vignes [16], dilatometric
		$\alpha^{+24+35}=14.1_6$	
5		$\alpha^{+10+35}=14.7_5\pm0.1$	Imai [17], dilatometric
6	$1.772_3/1.768_9$	$\alpha^{20^\circ\mathrm{C}}=12.8_6$	Jona [18]
7	$1.769_4/1.766_5$	$\alpha^{+20+35}=11.0_3$	Alexandru, this paper

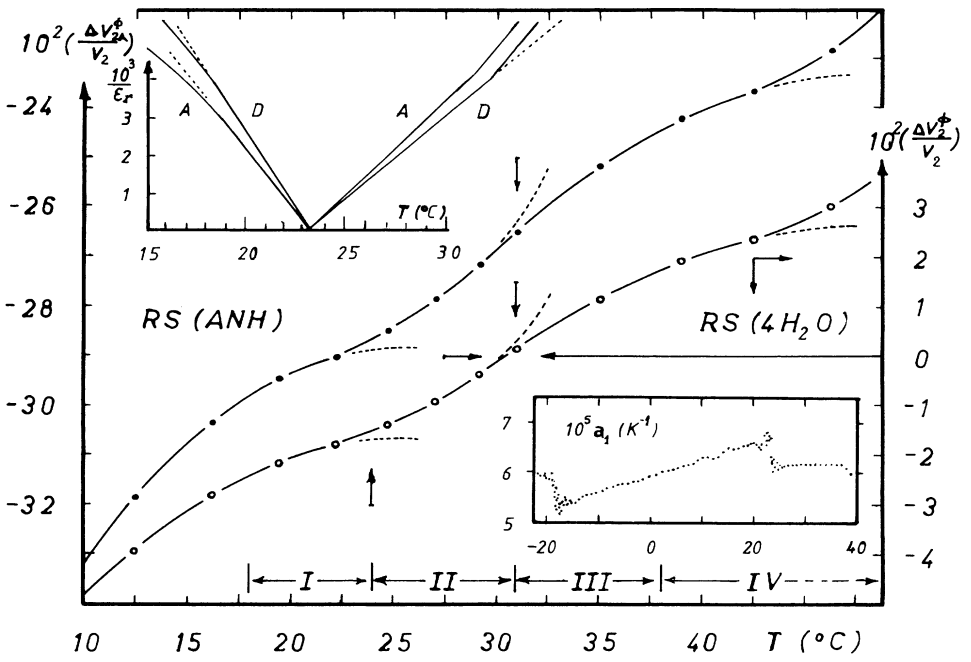

FIG. 3. The relative excess of the apparent volume of solute RS in solutions vs the saturation temperature. The lower curve RS·$4H_2O$ is for the hydrated solute. The upper curve RS(anh) is for anhydrous solute. The upper inset presents the reciprocal permittivity of the RS crystal according to Kawai [25] for *A* 80%, *D* 32% surrounding humidity. The lower inset presents the linear-expansion coefficient a_1 along the ferroelectric axis of the RS crystal according to Imai [17].

It is about constant on the II and III temperature ranges: $14.8_5\times10^{-5}$ °C^{-1}.

VII. APPARENT PARTIAL VOLUME OF SOLUTE IN SOLUTIONS

In order to get an idea about the microscopic state of solutions we have calculated the apparent specific volume of solute, considering the solvent water acting as in the pure state. First we have accounted the four cystallization water molecules of $NaKC_4H_4O_6\cdot4H_2O$ as being part of solute—curve RS ($4H_2O$) in Fig. 3—and second acting as a solvent—see curve RS (anh) in Fig. 3.

We have considered the solution volume (at the saturation point)

$$V_{\text{sol}}=n_2V_2^{\phi}+n_1V_1\ , \tag{10}$$

where V_2^{ϕ} is the apparent molar volume of solute, and n_2 and n_1 are the mole numbers of solute and solvent, respectively.

The specific volume v_2^{ϕ} (cm^3/g) could be calculated from the equation

$$v_2^{\phi}=\frac{1}{z_0}\left[\frac{1+z_0}{\rho_{\text{sol}}}-\frac{1}{\rho_1}\right], \tag{11}$$

where z_0 is the solubility (g solute/g solvent), ρ_1 is the density of pure water which depends on temperature [11], and ρ_{sol} is the saturation density of solution.

We have calculated the relative excess of the apparent volume of solute versus the volume in the solid state ($v_2=1/\rho_2$), from Eq. (8), using the formula

$$\frac{\Delta v_2^{\phi}}{v_2}=\frac{v_2^{\phi}}{v_2}-1=\frac{\rho_2}{z_0}\left[\frac{1+z_0}{\rho_{\text{sol}}}-\frac{1}{\rho_1}\right]-1\ . \tag{12}$$

The result is represented in Fig. 3, curve RS($4H_2O$).

We have calculated the other curve, RS(anh) in Fig. 3, according to the equation

$$\frac{\Delta v_{2A}^{\phi}}{v_2}=\frac{v_{2A}^{\phi}}{v_2}-1=\left[\frac{\Delta v_2^{\phi}}{v_2}+K\left[1-\frac{\rho_2}{\rho_1}\right]\right](1-K)^{-1}, \tag{13}$$

where $K=4M_{H_2O}/M_{RS\cdot4H_2O}$ (molar ratio). This last equation is not entirely correct as long as we take the excess volume Δv_{2A}^{ϕ} of the anhydrous salt versus the volume v_2 of the hydrated salt (the temperature dependence of the density of the anhydrous salt is unknown). So the second curve RS(anh) in Fig. 3 has to be considered only qualitatively.

Both curves in Fig. 3 present essentially the same features. Between the two bending points at 24 °C and 31 °C an opposite curvature is clearly seen, apparently not related to other physical parameters as yet.

The most interesting fact is that the excess volume of hydrated RS becomes zero around the saturation temperature 30.5 °C. This fact is also suggested by Ogawa calculations. We have estimated from his data (Table III in Ref. [20]) that at a temperature of about 31 °C the excess volume of the solute RS in solution is zero.

VIII. DIELECTRIC PROPERTIES OF RS SOLUTIONS

The temperature of the second-order transition, as revealed by density measurements of the RS solutions (Fig.

2), happens to be the upper Curie point of the ferroelectric transition in RS single crystals. If the quasicrystalline structure of solute is typically for the saturated solutions, then a ferroelectric component of permittivity in these solutions might be detectable. Some preliminary results of electrical measurements of the RS saturated solutions are presented here.

The RS basic substance that we used in these experiments was purified according to a special procedure previously applied for other substances [21]. The "middle" fraction of recrystallized substance and twice-distilled water (in quartz) were used for solutions preparation. A FERISOL Q-meter cell and 1-kHz bridge ($E=0.15$ V/cm) have been used to measure both the electrical capacity and the loss tangents of solutions. The temperature has been controlled (± 0.05 °C) by water circulation in the double walls of the cell from a standard thermostat.

In the temperature range 14–30 °C around the Curie point, measurements were performed for every Celsius degree and for every two Celsius degrees on 30–50 °C temperature range at different rates.

At each and every step the temperature of the cell becomes stable in 2–3 min. Three to five measurements could be safely performed towards the end of the steady-state time interval (median values have been retained).

The solutions permittivity (considered as proportional to the electrical capacity of the cell) increases rapidly with the temperature. Measured points fall on straight lines interrupted by decreasing jumps around some specific temperatures due to relaxation phenomena in solutions. Jumps were usually noticed around 20 °C and 30 °C. A small feature has been noticed around 24 °C over the base line, for every tested composition. However, the most prominent peak has been found for solution composition having 24 °C as the saturation temperature. We present experimental data for such a composition below.

In the $Q10$ experiment temperature has been *lowered down at a pace of 1 °C every 10 min.* In the $Q11$ experiment for the same solution (preserved 5 days in the cell) the temperature has been *increased 1 °C every 20 min.* Although the experimental points do not coincide in both experiments, their fitting curves follow the same pattern and are closely parallel to each other (electrode polarization at 1 kHz might still appear [22]).

The following equation has been used to fit the experimental data:

$$C(\mu\mathrm{F})=C_r+s(T-T_r)+\frac{K}{T-T_0}\ , \tag{14}$$

where C_r and T_r are the coordinates of a reference point around 20 °C, and s is the slope of the base line and the last term is a "ferroelectric" component to be discussed further. Results of the last term estimation ΔC_ϵ are presented in Fig. 4. At one Celsius degree apart from the "Curie point," the third term in Eq. (14) represents 15–30 % from the second one and this at its turn represents about 0.65% from the first one. It is a remarkable fact that this ferroelectric component obeys the Curie-Weiss law. Both experiments $Q10$ and $Q11$ have produced experimental $(\Delta C_\epsilon)^{-1}$ points falling on the same straight lines below and above the Curie point with a slope ratio 1.9. This ratio is close to 2 as predicted by the Landau theory of ferroelectrics [23,27] and is in reasonable agreement with experimental data of RS single crystals [24–28] (other experimental data show this ratio to be within 1.5–1.9).

Considering the electrolytic cell parameter (surface-to-gap ratio) to be about 400 cm, we estimate the overall solution permittivity to be $\epsilon_r^{\mathrm{sol}}=8.2\times 10^6$ [for $C_r\simeq 290$ μF in Eq. (14)] and the excess ferroelectric permittivity 1 °C apart from the Curie point 24 °C to be $\Delta\epsilon_r\simeq 10^4$ [for $K=(0.3\text{–}0.5_8)$ μF °C].

The overall permittivity value of 10^7 is unusually large due to the huge amount of dipoles that can switch more or less freely in solution under the action of the electric field. However, this figure is not unexpected if we keep in mind that the RS single crystal reaches $\epsilon_r\simeq 10^7\text{–}10^8$ at the melting point around 58 °C [9,28].

On the other hand, the ferroelectric component $\Delta\epsilon_r\simeq 10^4$ (almost at the limit of detection in our experiments) is very large and only comparable with the peak values of the RS crystal permittivity found in elaborate experiments [26].

Orientational polarization has the essential role versus the distortional one in the permittivity of solutions [22,29]. On the other hand, the imaginary part of permittivity $\epsilon''=\epsilon'\tan\delta$ is quite large, because $\tan\delta\leq 0.5$ (the conductive component could not be estimated in our ex-

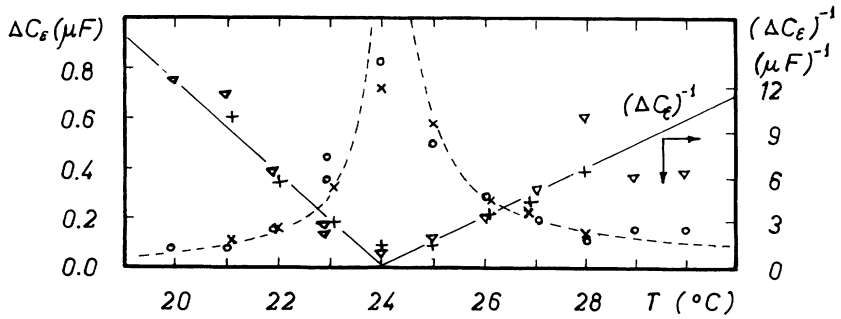

FIG. 4. The ferroelectric component of electrical capacity—the third term in Eq. (14)—and its reciprocal value for RS, 24 °C saturated solution. The $Q10$ experiment (temperature decreasing): ΔC_ϵ ($\times$), ΔC_ϵ^{-1} (+). The $Q11$ experiment (temperature increasing): ΔC_ϵ ($\circ$), ΔC_ϵ^{-1} (∇).

perimental conditions). The ferroelectric component of permittivity in RS saturated solutions can be considered as strong evidence of the existence of a solute quasicrystalline state.

IX. OTHER DATA

We shall approach first the solubility data of RS and then we shall calculate the dependence of the dissolution enthalpy values in the 10–50 °C temperature range. We consider the dissolution process as an equilibrium reaction between the solid substance and the solute in solution. The van 't Hoff isobar reaction equation is

$$\left[\frac{\partial \ln K}{\partial T}\right]_P = \frac{\Delta H}{RT^2} , \tag{15}$$

where we consider the equilibrium constant $K(P,T)$ in the first approximation as the ratio of concentrations in mole fractions. So $K(P,T)=X_2/1$ (X_2 is the mole fraction of solute in solution) because the concentration of solute in the other (solid) phase is one.

Equation (15) can be rewritten

$$\frac{\partial \ln X_2}{\partial(1/T)} = -\frac{\Delta H_d}{R} , \tag{16}$$

where the reaction enthalpy is the dissolution enthalpy ΔH_d. For two close solubility points a mean value can be calculated,

$$\frac{\Delta H_d}{R} = -\frac{\ln(X_2''/X_2')}{1/T''-1/T'} . \tag{17}$$

Generally, if we consider activities instead of concentrations, $a_2=X_2\gamma_2$, on a narrow temperature interval, where ΔH_d can be looked upon as constant, we find from Eq. (15)

$$\ln X_2 = -\frac{\Delta H_d}{RT} + \left[\frac{\Delta S}{R} - \ln\gamma_2\right] , \tag{18}$$

where we designate the last term in parentheses as $\Delta S_d/R$.

The dissolution enthalpy $\Delta H_d^{\text{RS anh}}/R$ and the dissolution entropy $\Delta S_d^{\text{RS anh}}/R$ have been calculated from Eqs. (17) and (18), according to the solubility data [7,8]. Both quantities have been plotted in Fig. 5.

The dissolution process can be imagined according to the following cycle: the solute is heated from temperature T, then is melted at the temperature T_m and undercooled again. In this metastable state the "liquid" solute is mixed isothermally at the temperature T with the solvent. The mixing enthalpy is written $\Delta H_{\text{mix}}-\Delta H_h$ so as to make evidence of the hydration enthalpy evolved in the last stage of the process.

The dissolution enthalpy is

$$\Delta H_d = \int_T^{T_m} (C_P^{(S)} - C_P^{(L)})dT + \Delta H_m + \Delta H_{\text{mix}} - \Delta H_h , \tag{19}$$

where ΔH_m, the melting enthalpy, together with the next term, shall be designated as $\Lambda_m(T_m)$. Usually the first term in Eq. (19) has a minor contribution and shall be

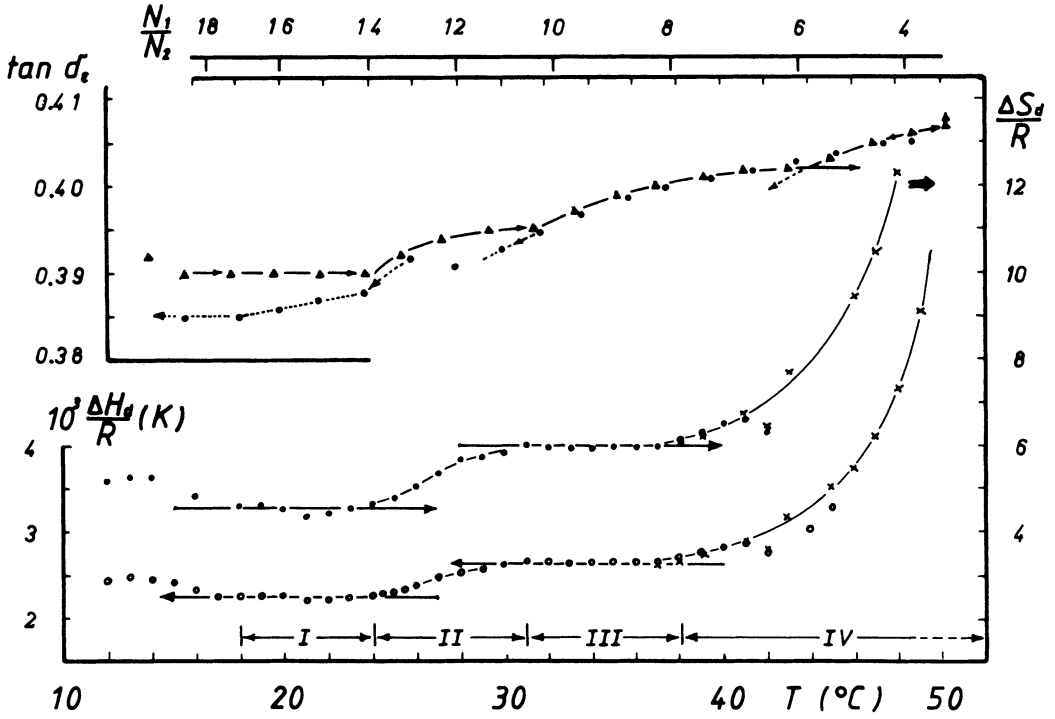

FIG. 5. The dissolution enthalpy $\Delta H_d^{\text{RS anh}}$ (○) and the dissolution entropy $\Delta S_d^{\text{RS anh}}$ (●) estimated from the solubility curve (see text). Top—the dielectric losses of $T_S=19$ °C, RS saturated solution from experiment *Q*5. The upper abscissa scale N_1/N_2 represents the number of water-solvent molecules "associated" with every RS·4H$_2$O solute molecule in solutions at different saturation temperatures (lower abscissa scale).

further neglected.

We have approximately for anhydrous and hydrated RS

$$\Delta H_d^{\mathrm{RS\,anh}} = \Lambda_m^{\mathrm{RS\,anh}}(?\,^\circ\mathrm{C}) - \Delta H_h^{X_1} - \Delta H_h^{4\mathrm{H_2O}} , \quad (20)$$

$$\Delta H_d^{\mathrm{RS\cdot 4H_2O}} = \Lambda_m^{\mathrm{RS\cdot 4H_2O}}(58\,^\circ\mathrm{C}) - \Delta H_h^{X_1} , \quad (21)$$

where $\Delta H_h^{4\mathrm{H_2O}}$ and $\Delta H_h^{X_1}$ are the hydration enthalpy for the inner solvation shell and for the outer solvation atmosphere, respectively.

The dissolution enthalpy $\Delta H_d^{\mathrm{RS\,anh}}$ in Fig. 5 has constant values on the distinct temperature intervals I and III,

$$\Delta H_d^{\mathrm{I}(18-24\,^\circ\mathrm{C})} = 4.5 \text{ kcal/mol} , \quad (22)$$

$$\Delta H_d^{\mathrm{III}(31-38\,^\circ\mathrm{C})} = 5.3 \text{ kcal/mol} . \quad (23)$$

The first value Eq. (22) is comparable, but somehow larger than 3.7_2 kcal/mol found by Ogawa [30] on a larger temperature range (apparently $-8, +30\,^\circ$C). The dissolution entropy $\Delta S_d^{\mathrm{RS\,anh}}$ mainly follows the same pattern as in Fig. 5.

X. SURVEY OF EXPERIMENTAL DATA

There are five sets of experimental data which relate to the I–IV temperature interval regularities.

(1) The volume-expansion coefficient α_s in Fig. 2 increases on the ranges I and III and decreases on the other ranges II and IV. We can write

$$\alpha_s = \frac{1}{V}\left[\frac{dV}{dT}\right]_{T_S} = \frac{1}{V}\left[\frac{dV}{dX_2}\right]_{T_S}\left[\frac{dX_2}{dT}\right]_{T_S} = \alpha_s^{X_2}(T_S)\frac{\Delta H_d}{RT_S^2}X_2(T_S) , \quad (24)$$

where Eq. (16) has been used to calculate $(dX_2/dT)_{T_S}$. The solubility curve $X_2(T_S)$ is smooth. The other factor $\Delta H_d/RT_S^2$ (see Fig. 5) does not match the α_s shape in Fig. 2. Only the solute can be considered responsible for the second-order transition: $\alpha_s \sim \alpha_s^{X_2}(T_S)$. Up to about 30 °C (I and II temperature intervals), the anomaly of the volume-expansion coefficient of solutions $\alpha_s(T_S)$ is related to the ferroelectric transition of the quasicrystalline RS·4H_2O solute.

(2) The relative excess of the solute volume, which we have plotted in Fig. 3, has been calculated using some other experimental data in Eqs. (11) and (12) than those used in Fig. 2. The main parameter responsible for the transition in Fig. 2, $(d\rho_s/dT)_{T_s}$, has not been used, so this sort of data can be considered as independent.

The normal curvature on ranges I and III is related to the stable configurations of solute in relation to the solvation enthalpy [see Fig. 5 and Eq. (20)]. The inverted curvature of $\Delta V_2^\phi/V_2$ on range II (Fig. 3) is related to the disordered paraelectric phase of solute at $T > T_c$. The temperature range IV with a similar inverted curvature in Fig. 3 corresponds to the disordered stage where RS·4H_2O starts to decompose in separate tartrate (see Sec. XII).

(3) Dielectric measurements of the saturated RS solutions show a ferroelectric component with a second-order transition, Fig. 4. This component obeys the Curie-Weiss law on both I and II temperature intervals. The RS single crystal has a perfect linear dependence of $1/\epsilon_r = f(T - T_c)$ on separate temperature intervals I (about 16–18 °C to 24 °C) and II (up to about 30–32 °C), where a clear bending sets the border of temperature range III [24,25,27,28]—(see the upper inset in Fig. 3). The slope of $1/\epsilon_r$ in region III exceeds by about 45% the similar slope on region II, as we have estimated from the experimental data of Kawai (Table I in Ref. [25]). This temperature of $\sim 31\,^\circ$C seems to point to the fact that a new stable configuration in the crystal lattice has been reached on temperature interval III.

This new stable configuration of the quasicrystalline solute is also remarkably shown in Fig. 5 by the constancy of the dissolution enthalpy ΔH_d on temperature interval III. This might show that the solvation enthalpy (mainly $\Delta H_h^{4\mathrm{H_2O}}$ of the first solvation shell) is about constant on this range, due to the stable configuration of the core RS·4H_2O [see Eq. (20)].

(4) The dissolution enthalpy $\Delta H_d^{\mathrm{RS\,anh}}$ (and also the dissolution entropy $\Delta S_d^{\mathrm{RS\,anh}}$) in Fig. 5 shows the state of solute in saturated solutions.

As NMR data shows, in other crystallohydrates the crystallization water molecules are deeply involved in the ferroelectric effect [31]. More than half of the spontaneous polarization (mainly the orientational component) can be assigned to the four hydration water molecules in deuterated RS crystals [32]. These molecules are stiffly bounded in the lattice below the Curie point. The whole system of hydrogen bonds changes during the order-disorder transition.

The volume-expansion coefficient α_v^{cr} of the RS crystal, as previously shown, has a small but defined discontinuity jump at the Curie point. On the other hand, the volume-expansion coefficient $\alpha_s(T_S)$ of solutions in Fig. 2 has a steeply remarkable decrease on temperature interval II obtained at the increasing of the solution concentration. This is correlated with the steep increase of ΔH_d dissolution enthalpy and the decrease of solvation enthalpy, Eq. (20). This in turn is correlated to an abnormal increase on range II of the apparent solute volume (Fig. 3) due to expansion of the solvation atmosphere.

Around the temperature of 31 °C the excess of the apparent solute volume (Sec. VII) becomes zero, showing an "ideal" behavior of components in solution. Indeed, around this temperature the number of water solvent molecules N_1/N_2 (upper abscissa scale in Fig. 5), which can be "associated" with every RS·4H_2O molecule, is about 10–12. We recall that in the close-packed crystal structures, the number of neighbors in the first coordination sphere is 12. On the III temperature range the outer solvation atmosphere becomes "transparent" enough so that the solute-solute interaction has the same value as the solute-solvent interaction.

On range IV of temperatures, which extends up to the melting point $\sim 58\,^\circ$C [33], the inner solvation shell is

gradually "disintegrated." A continuous decrease of all a_1, a_2, and a_3 linear-expansion coefficients of the RS crystal has been recorded by Imai [17] at temperatures higher than 36 °C (he referred to it as a plastic property—see the lower inset in Fig. 3). This shows that the crystallization water molecules are displaced from the crystal lattice on temperature range IV and the solute RS·4H_2O decomposes in separate tartrates. In solutions, on range IV, the dissolution enthalpy ΔH_d sharply increases, and the solvation enthalpy decreases almost in the same manner—Eq. (20).

(5) The dielectric losses of $T_s = 19$ °C saturated solution from the $Q5$ experiment have been plotted in Fig. 5. Measurements have been performed first by increasing the temperature up to 50 °C and then by decreasing it, at the same rate of 2 °C every 10 min. Experimental points fall on the same curve, except for the returning part below 32 °C, where it seems solution relaxation has not been achieved.

The shape of this $\tan\delta_\epsilon$ curve proves the real existence of the four well-defined temperature intervals. The border temperature value between ranges III and IV is, however, shifted towards ~44 °C, due to the lower concentration of this solution.

XI. SOLUTION DENSITY AND CRITICAL PHENOMENA

The basic response functions, i.e., the specific heat and the compressibility, measure the heat absorption from a temperature stimulus and the volume response to a pressure stimulus. Both functions are the second differential of the Gibbs free energy versus the temperature and the pressure, respectively. The third response function, the thermal-expansion coefficient, received less attention. At constant pressure we consider the volume-expansion coefficient along the solubility curve

$$\alpha_s = \frac{1}{V}\left(\frac{dV}{dT}\right)_{T_S} = -\frac{1}{\rho}\left(\frac{d\rho}{dT}\right)_{T_S} = \frac{1}{V}\left(\frac{\partial^2 G}{\partial P \partial T}\right)_{\text{solub curve}} \tag{25}$$

and we attempt an interpretation in the frame of the critical phenomena.

Because α_s does not diverge to infinity at the critical point, but it has rather a cusplike singularity or a jump discontinuity, we try to find the critical exponent in the equation suggested by Stanley for such situations (p. 41 in Ref. [23]),

$$\alpha_s = A - Bt^{\lambda}, \tag{26}$$

where $t = |1 - T/T_c|$ is the reduced temperature.

At the limit $t \to 0$, near the critical point $\alpha_s \to \alpha_{sc} = A$ if $\lambda > 0$, and Eq. (26) takes the normalized form

$$\left|1 - \frac{\alpha_s}{\alpha_{sc}}\right| = \mathcal{B}\left|1 - \frac{T}{T_c}\right|^{\lambda}. \tag{27}$$

We have considered the approach to T_c from the low-temperature side. The four points corresponding to α_s in Fig. 2 at $T < 24$ °C fitted the Eq. (27) in double logarithmic scale. For $\alpha_{sc} = 45.2 \times 10^{-5}$ °C^{-1} with a correlation factor $r = 99.9_2\%$, we found $\mathcal{B} = 0.98_2$ and the critical exponent $\lambda = 0.55$ (α_{sc} has been somehow arbitrarily chosen for the best fit of data; for $\alpha_{sc} = 45.0 \times 10^{-5}$ °C^{-1}, $r = 99.9_0\%$, $\mathcal{B} = 1.06_7$, and $\lambda = 0.58_3$). As expected for such a normalized representation $\mathcal{B}$ is close to one [23], while the critical-point exponent is close to $\frac{1}{2}$. Taking into consideration the fact that the solute RS in solution has many similar properties to the RS crystal and the heat capacity of the RS crystal has a small jump discontinuity [34,35] at 24 °C like other ferroelectrics have [36,23], our interpretation seems adequate.

XII. GENERAL DISCUSSIONS

It is recognized that the hydrated crystals grow much more easily from water solutions than the anhydrous ones. It is supposed that the flat faces of the crystals grown from solutions have an activated mechanism of growth. The highest potential barrier that has to be surpassed by the growth unity which enters from the bulk of solution into the adsorbed layer or directly into the kink on the crystal surface is the dehydration step [37–39]. For the sucrose crystal growth (having very large solubility like the RS, but anhydrous) from the Arrhenius plot, Bennema has found an activation energy of 15.7 kcal/mol [40].

For the RS crystal growth, using the same procedure, we have found (5±1) kcal/mol [3,5,41,42]. From other data Shiomi, Kuroda, and Ogawa [43] have found the "heat of crystallization" for the RS to be 4.3 kcal/mol, in reasonable agreement with our data. Experimental NMR data [44,45,20,46] for the RS solutions at 36 °C show that solute RS is in a very similar state to the crystalline one.

An activation energy larger than 12 kcal/mol (usually 15–25 kcal/mol) is estimated for the dehydration step in the growth process [5,38,39]. The activation energy for RS crystal growth of 5 kcal/mol, which is quite small, can be associated with the hydration enthalpy equation (21) of the outer solvation atmosphere $\Delta H_h^{X_1}$ of solute RS·4H_2O. This shows that only very few water molecules of the solvent are loosely bonded in this outer atmosphere, because their binding energy is equivalent to only one hydrogen-bond energy.

Now, because the whole hydration enthalpy, which can be assimilated to the activation energy for the growth of usual anhydrous crystals, is about 15–25 kcal/mol, the hydration enthalpy of the first solvation shell has to be much larger than that of the outer solvation atmosphere. This can explain the stability of the quasicrystalline structure of solute in solution.

The difference between the dissolution enthalpies [Eqs. (22) and (23)] $\Delta H_d^{III} - \Delta H_d^{I} \simeq 0.8$ kcal/mol is quite small versus the hydrogen bond of ~4.5 kcal/mol. It is comparable to $RT \simeq 0.6$ kcal/mol at room temperature, so there are some changes, thermally activated, in the core of solute RS·4H_2O. Similar changes take place probably in the RS crystal as shown by dielectric measurements (the bending of $1/\epsilon_r$ around 30–32 °C, Fig. 3, upper inset).

The constant value of ΔH_d^{III} on the III temperature range in Fig. 5 shows the decreasing number N_1/N_2 from 11 to 8 of the solvent molecules and does not make a significant contribution to the overall hydration enthalpy because the major part of this enthalpy is concentrated in the first solvation shell. The slow increase of the dielectric losses of $T_s = 19\,^{\circ}C$ saturated solution on this range might show a feeble "disintegration" of the outer solvation atmosphere which proceeds by increasing the temperature.

In temperature range IV the sharp increase of the dissolution enthalpy (Fig. 5) shows the inner solvation shell is now progressively disintegrated. The overall hydration enthalpy $\Delta H_h^{4H_2O} + \Delta H_h^{X_1}$ in Eq. (20) sharply decreases on this range, mainly on account of the inner solvation shell. This effect is quite obvious in Fig. 5.

Indeed, starting from about 38–42 °C, the $RS{\cdot}4H_2O$ solute progressively decomposes in solution in separate tartrates according to the equation

$$2\,NaKC_4H_4O_6{\cdot}4H_2O \rightleftarrows Na_2C_4H_4O_6{\cdot}2H_2O + K_2C_4H_4O_6{\cdot}\tfrac{1}{2}H_2O + 5\tfrac{1}{2}H_2O \ . \quad (28)$$

In our experiment at 46 °C saturation temperature, the solute is partly decomposed and the Na_2 tartrate, being less soluble, has the tendency to fall down in solution.

Solvation is related to the Coulomb interaction between the ions and the solvent dipolar molecules; the involved energy is larger than the bonding energy of the solvent molecules. An average number of solvent molecules (but not specific individual molecules) are associated with a particular ion for a defined period of time, depending on the temperature and solution concentration [47,48].

Small single (or multicharged) ions Li^+,Na^+,Ca^{2+} have a very strong interaction with the water solvent molecules at short distances, which increases the solution viscosity and decreases the mobility and the rate of exchange of the solvent molecules in their vicinity. They are said to be positively solvated. The large singly charged ions K^+, Cs^+ are negatively solvated, thus having the opposite effect [49]. Solvation usually makes new ordered structures and diminishes ion-dipole volume (temperature ranges I and II in Fig. 3).

A pictorial image is the dynamic solvation of ions which moves through the relatively unstructured solvent. They are accompanied by an "atmosphere" of loosely bounded solvent, whose molecules are continually exchanging from the periphery with the unbounded solvent [50]. In the first solvation shell, solvent molecules can be considered as firmly bound and completely oriented. The primary hydration number (water molecules) for monovalent cations is $Li^+ = 4.0$, $Na^+ = 3.1$, $K^+ = 2.1$, $Rb^+ = 1.6$, $Cs^+ = 1.0$ (p. 159 in Ref. [50]).

Testing the RS crystal structure with this view, as presented by Beevers and Hughes [15] in (001) projection, we come to the conclusion that Na^+ and K^+ ions retain in the lattice the same primary hydration number of water molecules as in the solution. Indeed, as seen in Fig. 6, the Na^+ ion in an octahedral arrangement keeps three water molecules close (7, 2.39 Å, 8, 2.34 Å, and 10, 2.31 Å); the K^+ ion in a tetrahedral configuration has two water molecules of the same type (9, 3.01 Å) and in the other position keeps two water molecules close (7, 2.75 Å) (the other two water molecules 8, 3.07 Å, are at a larger distance).

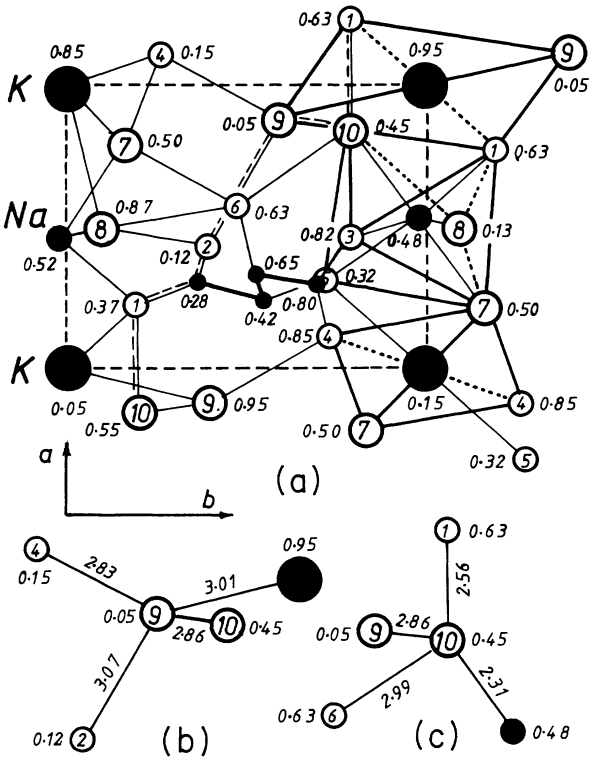

FIG. 6. One-quarter of the RS crystal cell, following Beevers and Hughes x-ray structure [15]. (a) The first coordination sphere of Na and K atoms in the lattice (our interpretation—see text). (b) and (c) The tetrahedral configuration around water molecules 9 and 10 supposed to be weakly bounded in the lattice. (1–6 smaller circles are O or OH.)

The octahedral configuration seems to be quite stable due to Na^+ positive solvation. Cu^{2+} substituted for Na^+ in a RS:Cu impurified crystal have the same configuration [51] and the ferroelectric properties are little affected by depressing the upper Curie point. The other substitution K^+ ion with a 1.33-Å radius, by a Rb^+ ion with a 1.49-Å radius in the lattice, has major implications. About 2 mol % rubidium completely suppresses ferroelectric properties of the impurified RS crystal [52,53] (ammonium and thallium replacing potassium in the lattice [15] have the same effect).

This behavior can be related to the primary hydration number 1.6 for Rb^+ which is less than 2.1 for K^+. This in turn points to the binding energy of the 9 water molecule in the lattice. The Bernal-Fowler tetrahedral configurations around water molecules 9 and 10 are presented in Figs. 6(b) and 6(c).

According to Beevers and Hughes [15], the chain of atoms 1-10-9-2-1-10 with reversible polarizability is responsible for the ferroelectric effect in the RS crystal

[Fig. 6(a)]. However, the weak point of the chain is the water molecule 9. It is loosely bound in the lattice, because the 3.07-Å distance to the oxygen 2 is at the limit of the H bridge and, on the other hand, the negative solvation of the potassium atom K, 3.01 Å, might show another weak bond (in the other position, the potassium atom has 2.75 Å to the 7 water molecule.

The water molecules 9 and 10 have been supposed to influence as defect sites in the distribution of the relaxation times in dielectric measurements at low frequencies [52]. Besides, the water vacancies homogeneously distributed in the crystal volume change the Curie temperature and the permittivity, both in the ferroelectric and paraelectric phases [24–26,52,54].

If the hypothesis of Beevers and Hughes [15] about the ferroelectric mechanism in RS crystal is correct, our supposition is that the weak H bond 2—9 is broken probably at the Curie point 24 °C and a disordered state in the lattice follows on the temperature range II, in the paraelectric phase, next to the transition. It seems quite probable that the water molecule 10 is simultaneously disturbed, but a quasistable configuration seems to be achieved on the III temperature range.

On approaching the Curie point from the lower temperature side, the continuous increase of a_1, the linear-expansion coefficient along the ferroelectric axis of the crystal (lower inset in Fig. 3), shows that a nonlinear abnormal extension takes place in the lattice (and a simultaneous contraction in the other two directions). After the breaking of the 2—9 H bonds at the Curie point along the ferroelectric axis, the linear coefficients a_1, a_2, a_3 of the crystal become almost constant on the next II and III temperature ranges. In solutions, due to increasing interaction between the solute particles by increasing concentration (and decreasing solvation), some related effects appear as already shown.

In temperature range IV, Na^+ retains in close proximity only two water molecules, probably 7 and 8, as decomposition proceeds in separate tartrates, Eq. (28). In this range all linear-expansion coefficients of the crystal decrease; the volume-expansion coefficient of solutions decreases with concentration as well.

Finally we discuss solution electrical measurements and some other implications. The Curie-Weiss law for the ferroelectric component of solution permittivity could be followed only about ±4 °C around the Curie temperature 24 °C due to the limited accuracy (a double temperature interval is covered for the RS crystal—upper inset in Fig. 3).

The narrow temperature interval around the Curie point, where the Curie-Weiss law is not verified (usually called the nonclassical behavior), is about 1 °C in RS solutions, while in the crystal it is less than 0.1 °C [26]. Although the maximum value of the ferroelectric component represents only about 2×10^{-3} from the overall solution permittivity, its absolute value of 10^4 is very large and is comparable with the top values found for single crystals. This component brings evidence of the short-range order in solution and at the same time proves the quasicrystalline structure of solute.

XIII. CONCLUSIONS

(1) The quasicrystalline structure of RS solute and the ferroelectric properties associated with the saturated solutions have been proved. Similar properties of the crystal and solute RS in solutions have been pointed out on the four temperature ranges between approximately 16 °C and the melting point of the crystal. Five types of experimental data give evidence about the specific properties of the crystal and solute on distinct temperature ranges, as follows.

(2) The volume-expansion coefficient $\alpha_s(T_S)$ of solutions (i.e., the second differential of the Gibbs free energy) undergoes a second-order transition around 24 °C versus the saturation temperature, along the solubility curve (Fig. 2). The jump discontinuity of this response function has been interpreted in the frame of the critical phenomena Eq. (27). The critical point exponent has been found to be close to $\frac{1}{2}$.

(3) The apparent partial volume of solute in solution shows a sort of "disordered" state on ranges II (24–31 °C), related to the ferroelectric transition, and IV (40–58 °C), related to the decomposition into separate tartrates, Figs. 3 and 5.

(4) The permittivity measurements of saturated solutions give evidence about the ferroelectric component related to the second-order transition, which obeys the Curie-Weiss law on temperature ranges I and II (Fig. 4).

(5) The dissolution enthalpy and the dielectric losses give clear evidence for the temperature ranges I–IV. We consider the increase of the dissolution enthalpy $\Delta H_d^{\mathrm{RS\,anh}}$ on the II (24–31 °C) temperature range to be related to the configurational changes in the $RS\cdot 4H_2O$ core of solute, reflected via the hydration enthalpy $\Delta H_h^{4H_2O}$, Eq. (20), Fig. 5.

(6) The examination of the x-ray crystal structure shows the solute RS joins the crystal lattice with the first solvation shell. Both Na^+ and K^+ ions have in the first coordination sphere in the lattice the same number of water molecules as the primary hydration numbers in solutions, Fig. 6(a). In the Beevers and Hughes crystal structure [15] the octahedral configuration around Na^+ seems to be much more stable and water molecules 7 and 8 to be firmly bound. Molecule 9 is loosely bound in the lattice and we suppose the weak H bridge 2–9 is broken off around 24 °C—the Curie point [Figs. 6(b) and 6(c)]. Water vacancies in the crystal are usually related to molecule 9 of water.

(7) For crystal-growth purposes, the solution-density data versus temperature and composition are of great importance. The saturation temperature of the growing solution (and hence the supersaturation) can be easily determined with less possible perturbations of the system if we measure the actual density ρ_{act} of the solution accurately enough (inset in Fig. 1).

[1] H. V. Alexandru, J. Cryst. Growth **8**, 115 (1969).
[2] H. V. Alexandru, Rev. Roumaine Phys. **4**, 241 (1974).
[3] H. V. Alexandru, Krist. Tech. **8**, 803 (1973).
[4] H. V. Alexandru and C. Motoc, Rev. Roum. Phys. **17**, 450 (1972).
[5] H. V. Alexandru, Ph.D. thesis, University of Bucharest, 1974 (in Rumanian).
[6] H. V. Alexandru, Proceedings of the Conference on Electrooptical Crystals and Liquid Crystals in Science and Industry, Lodz, Poland, 1973 (unpublished), p. 9.
[7] Ju. Lurie, *Handbook of Analytical Chemistry* (Mir, Moscow, 1975).
[8] I. Smid, J. Kvapil, J. Myl, and S. Solz, *Growth of Crystals* (Consultants Bureau, New York, 1962), Vol. 3.
[9] H. V. Alexandru (unpublished).
[10] H. V. Alexandru, J. Cryst. Growth **10**, 151 (1971).
[11] N. E. Dorsey, *Properties of Ordinary Water Substance* (Hafner, New York, 1968).
[12] N. A. Pratten, J. Mater. Sci. **16**, 1734 (1981).
[13] R. L. Kroes and D. Reiss, J. Cryst. Growth **69**, 414 (1984).
[14] A. R. Ubbelohde and I. Woodward, Proc. R. Soc. London Ser. A **185**, 448 (1946).
[15] C. A. Beavers and W. Hughes, Proc. R. Soc. London Ser. A **177**, 251 (1941).
[16] I. Vignes, Phys. Rev. **48**, 198 (1935).
[17] K. Imai, J. Pys. Soc. Jpn. **41**, 2005 (1976).
[18] F. Jona, Helv. Phys. Acta **XXIII**, 795 (1950).
[19] *Ferroelectric and Related Substances,* edited by K.-H. Hellwege and A. M. Hellwege, Landolt-Börnstein Vol. 16 (Springer-Verlag, Berlin, 1982).
[20] T. Ogawa (unpublished).
[21] H. V. Alexandru, A. C. Otea, and G. Hlevca, Rev. Roum. Phys. **30**, 525 (1985).
[22] N. E. Hill *et al.*, *Dielectric Properties and Molecular Behavior* (Van Nostrand, Princeton, 1969).
[23] H. E. Stanley, *Introduction to Phase Transitions and Critical Phenomena* (Clarendon, Oxford, 1971).
[24] H. Mueller, Phys. Rev. **47**, 175 (1935); **57**, 829 (1940).
[25] H. Kawai, J. Phys. Soc. Jpn. **3**, 105 (1948).
[26] G. Weissbach and H. E. Müser, Phys. Status Solidi **13**, 45 (1966).
[27] F. Jona and G. Shirane, *Ferroelectric Crystals* (Pergamon, New York, 1962).
[28] E. Watzlawec, M.S. graduation paper, Bucharest University, 1988.
[29] H. V. Alexandru, *Materials Science and Technology* (Bucharest University Press, Bucharest, 1990) (in Rumanian).
[30] T. Ogawa, Jpn. J. Appl. Phys. **16**, 689 (1977).
[31] H. Kiriyama and R. Kiriyama, J. Phys. Soc. Jpn. Suppl. **28**, 114 (1970).
[32] J. L. Bjorkstam, J. Phys. Soc. Jpn. Suppl. **28**, 101 (1970).
[33] W. G. Cady, *Piezoelectricity* (McGraw-Hill, New York, 1946).
[34] A. J. C. Wilson, Phys. Rev. **54**, 1103 (1938).
[35] J. Helwig, Ferroelectrics **11**, 471 (1976); **7**, 225 (1974).
[36] L. P. Kadanoff *et al.*, Rev. Mod. Phys. **19**, 395 (1967).
[37] W. K. Burton, N. Cabrera, and F. C. Frank, Philos. Trans. R. Soc. London Ser. A **243**, 299 (1951).
[38] P. Bennema *et al.*, Krist. Tech. **8**, 659 (1973).
[39] P. Bennema, J. Cryst. Growth **1**, 278 (1967).
[40] P. Bennema, J. Cryst. Growth **3,4**, 331 (1968).
[41] H. V. Alexandru (unpublished).
[42] H. V. Alexandru and I. Dima, An. Univ. Bucuresti Fiz. **30**, 65 (1981).
[43] Y. Shiomi, T. Kuroda, and T. Ogawa, J. Cryst. Growth **50**, 397 (1980).
[44] T. Ogawa and K. Satoh, J. Chem. Eng. Data Berlin, **21**, 33 (1976).
[45] T. Ogawa *et al.*, J. Cryst. Growth **56**, 151 (1982).
[46] T. Ogawa, Jpn. J. Appl. Phys. **16**, 689 (1977).
[47] J. P. Hunt, *Metal Ions in Aqueous Solution* (Benjamin, New York, 1963).
[48] R. G. Pearson and P. C. Ellgen, in *Reactions in Condensed Phase,* edited by H. Eyring, Physical Chemistry Vol. VII (Academic, New York, 1975).
[49] O. Ya. Samoilov, *Structure of Aqueous Electrolyte Solutions* and *Hydration of Ions* (Consultants Bureau, New York, 1965).
[50] E. S. Amis and J. P. Hinton, *Solvent Effects on Chemical Phenomena* (Academic, New York, 1973), Vol. 1.
[51] M. Schara and M. Sentjuc, Fizica (Beograd) **1**, 159 (1969).
[52] J. Pottharst, J. Phys. Soc. Jpn. Suppl. **28**, 439 (1970).
[53] R. S. Krishnan *et al.*, J. Phys. Soc. Jpn. Suppl. **28**, 167 (1970).
[54] H. G. Unruh and E. Sailer, Z. Phys. **224**, 45 (1969).